

Quantized two terminal conductance, edge states and current patterns in an open geometry 2-dimensional Chern insulator

Junaid Majeed Bhat¹, R Shankar², and Abhishek Dhar¹

¹International Centre for Theoretical Sciences, Tata Institute of Fundamental Research, Bengaluru 560 089, India,

²The Institute of Mathematical Sciences, C I T Campus, Chennai 600 113, India

(Dated: January 15, 2024)

The quantization of the two terminal conductance in 2D topological systems is justified by the Landauer-Buttiker (LB) theory that assumes perfect point contacts between the leads and the sample. We examine this assumption in a microscopic model of a Chern insulator connected to leads, using the nonequilibrium Green's function formalism. We find that the currents are localized both in the leads and in the insulator and enter and exit the insulator only near the corners. The contact details do not matter and a perfect point contact is emergent, thus justifying the LB theory. The quantized two-terminal conductance shows interesting finite-size effects and dependence on system-reservoir coupling.

Introduction: The quantum Hall effect (QHE) was discovered by von Klitzing [1] in 1980. Topological properties were invoked to understand why the Hall conductance was so exactly quantized in units of e^2/h . In a seminal paper, Thouless and others (TKNN) [2] identified the Chern invariant, ν , with the Hall conductivity, $\sigma_H = \nu e^2/h$. Hatsugai [3] showed that a non-zero Chern invariant, ν , of the closed system implies the existence of ν chiral edge channels in systems with edges. Chiral edge channels are central to the physics of insulators with non-trivial topology in two dimensions. They carry dissipationless current and are, to a certain degree, robust towards symmetry preserving disorder. Apart from quantum hall systems, several other insulators with non-trivial topologies have been discovered, namely those having non-zero Chern invariants without a magnetic field, the so-called Chern insulators (CI) [4–6] and time reversal invariant insulators with non-trivial Z_2 invariants, the so-called topological insulators (TI) [7–14]. Topological invariants have also been defined for closed aperiodic systems such as quasi-crystals and amorphous systems, characterized by the so-called Bott index [15–17]. All these systems are characterized by chiral edge channels that provide the experimental signature of the non-trivial topology. The fact that the edge channels are dissipationless leads to the possibility of applications in devices [18]. There is growing activity in this field, so-called topological electronics, which involves engineering the edge channels.

Topological invariants are defined only for closed periodic systems, whereas experiments are typically done in open systems coupled to leads, where the current is injected/ejected. In a Hall bar geometry, the probes are away from the leads. Thus the Hall conductance, G_H , and the longitudinal conductance, G_L measured in the Hall bar geometry may not depend on the details of the coupling to the leads. If the Green-Kubo results are assumed to hold in an open system, the TKNN result predicts that G_H is quantized and $G_L = 0$. Decades of experiments on QHE systems have confirmed these

predictions. For 2-dimensional TIs it has been proposed [8, 13, 19] that the signal of a non-trivial Z_2 invariant is the quantization of the *two-terminal* conductance, G . This prediction is based on theoretical models using the Landauer-Buttiker (LB) formalism, which assumes perfect transmission via point contacts from the leads to the edge channels [8, 19, 20]. It is not theoretically obvious that the assumption of perfect transmission via point contacts is physically valid and follows from a microscopic approach such as the non-equilibrium Green's function (NEGF) formalism, where the leads are coupled to the system across its width and the transmission is explicitly related to details of both the reservoir model and its coupling with the system. This is the “theory gap” that is addressed in this work.

Since the topological properties of a 2-dimensional TI can be modelled as those of two decoupled CI's with opposite Chern numbers, we consider the strip geometry of a CI connected to metallic leads at two opposite edges, with a voltage difference V applied across the leads. Here one can measure not only G_H but also the two-terminal longitudinal conductance G , which is the main focus of this paper. Within the LB formalism it is easy to show that G is the same as G_H [19, 21].

In this Letter, we attempt to arrive at a better understanding of the two-terminal longitudinal conductance, G , in the open system by use of the NEGF formalism. For our studies, we consider the spinless BHZ (SBHZ) model [22], a Chern insulator, placed in contact with two metallic leads. Apart from measuring the conductance obtained from NEGF, we use this formalism to also extract information on the scattering states formed by the edge modes *in the presence of the leads*. The strip geometry makes this a highly non-trivial problem. In particular, for the scattering states, we obtain the current and charge density profiles inside the insulating region as well as in the metallic leads.

We summarize our main findings: we verify that G is quantized when the Fermi level is in the band gap of the insulator, and this is independent of the strength of the

coupling as well as any disorder at the contacts between the system and leads. This holds for sufficiently large system sizes while we find interesting finite size effects including oscillations whose period shows a simple scaling with the system size and the coupling strength. As expected, we find that the current in the CI is localized along the edges of the sample. Remarkably, the topological effect is felt even deep in the leads. For the case with the Fermi level set exactly at the middle of the gap, we find that the current is highly localized even in the leads, moving along a zig-zag line at 45° to the longitudinal direction (see Fig. (3)). The current only enters and leaves the insulator near the diagonally opposite corners, despite the fact that the reservoirs are coupled to the insulator throughout its width. This justifies the emergence of the perfect point contact, which is the main assumption of the LB formalism. As the Fermi level is shifted from the middle of the gap, the current density is less sharply localised but the injection(ejection) to(from) the CI is still near the corners [21].

The Model: The SBHZ model is a simple 2D topological insulator given by a nearest neighbor tight-binding Hamiltonian on an $N_x \times N_y$ rectangular sample. At any lattice point (x, y) , there are two fermionic degrees of freedom described by the annihilation operators $\psi_1(x, y)$ and $\psi_2(x, y)$, respectively. The Hamiltonian of the insulator is given by,

$$\begin{aligned} \mathcal{H}_W &= \sum_{x,x'=1}^{N_x} \sum_{y,y'=1}^{N_y} \Psi^\dagger(x, y) H_W[x, y; x', y'] \Psi(x', y'), \quad (1) \\ &= \sum_{x=1}^{N_x} \sum_{y=1}^{N_y} \mu_w \Psi^\dagger(x, y) \sigma_z \Psi(x, y) \\ &+ \sum_{x=1}^{N_x-1} \sum_{y=1}^{N_y} \left[\Psi^\dagger(x, y) \frac{1}{2} (\sigma_z + i\sigma_x) \Psi(x+1, y) + \text{h.c.} \right] \\ &+ \sum_{x=1}^{N_x} \sum_{y=1}^{N_y-1} \left[\Psi^\dagger(x, y) \frac{1}{2} (\sigma_z + i\sigma_y) \Psi(x, y+1) + \text{h.c.} \right], \end{aligned}$$

where we have defined the two-vectors $\Psi(x, y) = (\psi_1(x, y) \ \psi_2(x, y))^T$. The topologically non-trivial phases of Chern number 1 and -1 lie in the parameter regimes of $-2 < \mu_w < 0$ and $0 < \mu_w < 2$, respectively. In these parameter regimes, the rectangular sample with edges supports dissipationless edge modes with energies that lie within the gap of the insulator.

To study the transport due to the edge modes, we consider the system in contact with two external reservoirs at the two opposite edges at $x = 1$ and $x = N_x$. Each reservoir is taken to consist of two decoupled layers of metallic leads that are semi-infinite in the x -direction and of width N_y in the y -direction and are modelled as 2D nearest neighbour tight-binding Hamiltonians with hopping η_b (see [21]). The contacts between the edges of the

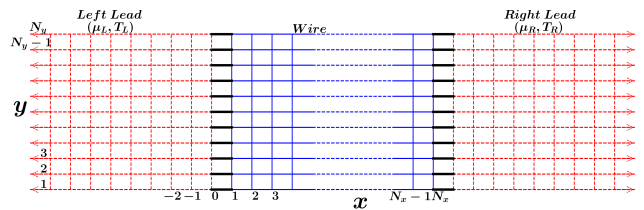


FIG. 1. Schematic of our strip geometry setup with a SBHZ CI in contact with two metallic leads

wire and the reservoirs are themselves modelled as tight-binding Hamiltonians with a uniform hopping strength of η_c [see Fig (1a)].

Using NEGF one can obtain the non-equilibrium steady state of this system starting from a state where the left and the right reservoirs are described initially by grand canonical ensembles with chemical potentials and temperatures (μ_L, T_L) and (μ_R, T_R) while the wire is in an arbitrary state. The non-equilibrium steady state solution for the wire operators in the limit $t \rightarrow \infty$ can be derived in terms of the effective Green's function of the wire given by $\mathcal{G}(\omega) = (\omega - H_W - \Sigma_L(\omega) - \Sigma_R(\omega))^{-1}$, where $\Sigma_{L/R}(\omega)$ are the self energies from the reservoirs [21]. From this solution, particle and heat currents and, in fact, all two-point correlators can be derived [23, 24]. We are interested in the conductance, and the profiles of charge density and the current density in the wire (including in the reservoirs) for the zero-temperature case, in the linear response regime ($\mu_L = \mu + \Delta\mu_L$ and $\mu_R = \mu + \Delta\mu_R$, with $\Delta\mu_L, \Delta\mu_R \ll \mu$).

The total current passing through the CI, in units of e^2/h , is given by $I = G(\mu)(\Delta\mu_L - \Delta\mu_R)$, where $G(\mu) = 4\pi^2 \text{Tr}[\mathcal{G}(\mu)\Gamma_R(\mu)\mathcal{G}^\dagger(\mu)\Gamma_L(\mu)]$ is the two-terminal conductance of the CI and $\Gamma_{L/R}(\mu) = [\Sigma_{L/R}(\mu) - \Sigma_{L/R}^\dagger(\mu)]/(2\pi i)$. The expressions for the current density can be computed from the correlation matrix, C with components given by $C[x, y, a; x', y', b] = \langle \psi_a^\dagger(x, y) \psi_b(x', y') \rangle$ with $a, b = 1, 2$ and the expectation value is taken in the non-equilibrium steady state. Using NEGF, C can be expressed in terms of the effective Green's function $\mathcal{G}(\omega)$ and the Fermi functions of the reservoirs [21].

The NEGF formalism can be reformulated to also compute the current density in the leads. The main idea is to use a setup where we include a part of the leads in the system Hamiltonian (see [21] for details). The current density in any finite segment of the new setup will be identical to the original setup because of uniqueness of the NESS.

As shown in [21], at $T = 0$ and in the linear response regime, the current on any bond between sites $\mathbf{x} = (x, y)$ and $\mathbf{x} + \mathbf{e}_s$, with $\mathbf{e}_1 = (1, 0)$, $\mathbf{e}_2 = (0, 1)$, can be written

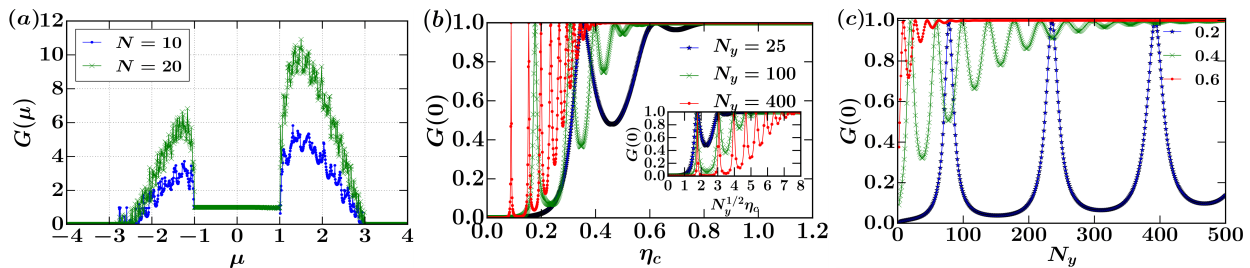


FIG. 2. In (a) we show the variation of the conductance with the Fermi level, μ . (b) and (c) show the variation of the conductance at the Fermi level, $\mu = 0$, with η_c and N_y at $N_x = 100$, respectively. The inset in (b) shows that, on scaling η_c with $N_y^{1/2}$, the peaks in the oscillations coincide and therefore the period of the oscillations scales as $N_y^{1/2}\eta_c$. Parameter values: (a) $N_x = N_y = N$, $\eta_b = 2$, $\mu_w = 1$, $\eta_c = 1.5$ and for (b) and (c) $N_x = 100$ $\eta_b = 2$ and $\mu_w = 1$.

as

$$J_{\mathbf{x},\mathbf{e}_s} = J_{\mathbf{x},\mathbf{e}_s}^{\text{eq}} + \bar{J}_{\mathbf{x},\mathbf{e}_s}^L + \bar{J}_{\mathbf{x},\mathbf{e}_s}^R, \text{ where} \quad (2)$$

$$J_{\mathbf{x},\mathbf{e}_s}^{\text{eq}}(\mu) = \int_{-\infty}^{\mu} d\omega [F_{\mathbf{x},\mathbf{e}_s}^L(\omega) + F_{\mathbf{x},\mathbf{e}_s}^R(\omega)], \quad (3)$$

$$\bar{J}_{\mathbf{x},\mathbf{e}_s}^L = F_{\mathbf{x},\mathbf{e}_s}^L(\mu)\Delta\mu_L, \quad \bar{J}_{\mathbf{x},\mathbf{e}_s}^R = F_{\mathbf{x},\mathbf{e}_s}^R(\mu)\Delta\mu_R, \quad (4)$$

where the functions $F_{\mathbf{x},\mathbf{e}}^{L,R}$ are defined in [21]. We call $\bar{J}_{\mathbf{x},\mathbf{e}_s} = \bar{J}_{\mathbf{x},\mathbf{e}_s}^L + \bar{J}_{\mathbf{x},\mathbf{e}_s}^R$ as the excess current density on the bond $(\mathbf{x}, \mathbf{e}_s)$ and $I = \sum_{y=1}^{N_y} \bar{J}_{x,y,\mathbf{e}_1}$ would give the nonequilibrium transport current across the CI. For points \mathbf{x} in the metal, $J_{\mathbf{x},\mathbf{e}}^{\text{eq}}(\mu) = 0$ for any μ , which implies that $F_{\mathbf{x},\mathbf{e}}^L(\mu) = -F_{\mathbf{x},\mathbf{e}}^R(\mu)$. However for points inside the CI, the topological phases support edge currents even in equilibrium, meaning that $J_{\mathbf{x},\mathbf{e}}^{\text{eq}}(\mu)$ is non-vanishing on the edges, consequently $F_{\mathbf{x},\mathbf{e}}^L(\mu) \neq -F_{\mathbf{x},\mathbf{e}}^R(\mu)$. This leads to the interesting observation that the excess current density in the CI does not simply change sign when we interchange $\Delta\mu_L$ and $\Delta\mu_R$ (though the total current $I = G(\Delta\mu_L - \Delta\mu_R)$ has this property). Note that the total current across any transverse cross-section vanishes, as expected in equilibrium. We emphasize that the excess current, \bar{J} , is a relatively small correction over J^{eq} , and is the transport current arising due to the chemical potential difference between the reservoirs. Only the total current density is expected to respect the chirality of the Chern insulator, while the excess current density can flow opposite to the chirality of the insulator since it is proportional to $\Delta\mu_{L/R}$. With similar arguments the excess charge density, $\bar{\rho} = \rho - \rho^{\text{eq}}$, where ρ^{eq} is the charge density for $\Delta\mu_L = \Delta\mu_R = 0$, can be expressed in terms of the correlation matrix C (See Eq. (S9) in [21]). We now present numerical results for the conductance $G(\mu)$ and the excess current density profiles.

Numerical Results: For the SBHZ wire, the edge modes lie within the gap, we therefore always set μ to be within the gap of the insulator. In Fig. (2), we plot the conductance as a function of the Fermi level, μ , for two system sizes. It is seen that when the Fermi level lies in the gap, the value of the conductance (in units of e^2/h) is

quantized to the value 1. In Fig. (2b,2c) we show the variation of the conductance, at Fermi level $\mu = 0$, with the strength of the coupling with the reservoirs, η_c , and the width of the insulator, N_y , respectively. From these plots, we see that the conductance strength approaches the quantized value and eventually becomes independent of η_c and N_y . The approach to the quantized value is oscillatory, with exact quantization being achieved at some specific values of η_c and N_y . The inset of Fig. (2b) shows, remarkably, that the oscillation period scales as $N_y^{1/2}\eta_c$.

Next, in Fig. (3a), we show the excess current density at zero Fermi level inside the insulator and the normal metallic regions with $\Delta\mu_L > 0$ and $\Delta\mu_R = 0$. We see that the current flows along the edges of the insulator, and the charge density is also localized along the edges [See Sec. III in [21]], as expected. Surprisingly, the excess current density is sharply localized even in the normal metallic regions. We see that the current primarily flows along the lines at 45 degrees to the horizontal direction and gets multiply reflected until it reaches the top corner of the SBHZ wire. At this corner, it gets injected into the insulator, flows along the edges and then leaves it at the diagonally opposite corner into the normal metallic region on the other end. The current density patterns inside the Chern insulator are sensitive to the choice of $\Delta\mu_L$ and $\Delta\mu_R$. This is due to that fact that $\bar{J}^L \neq -\bar{J}^R$ unlike in the metal. We illustrate this in Fig. (3b) which shows the current density pattern for $\Delta\mu_L = -\Delta\mu_R = \Delta\mu$. The current gets injected and ejected from the diagonally opposite corners as in Fig. (3a). However, it now flows along all edges of the CI which is different from Fig. (3a) where it flows only along two of the adjoining edges of the CI. Note that the current density along the opposite edges have opposite chirality, illustrating that the excess current can flow opposite to the chirality of the CI.

The features of the current density (corner injection and localization in the leads) are sharpest when the Fermi surface of the metal is a square in momentum space and smoothly fade away as the Fermi surface is deformed. In Sec. (IV) of [21], we illustrate this by presenting numer-

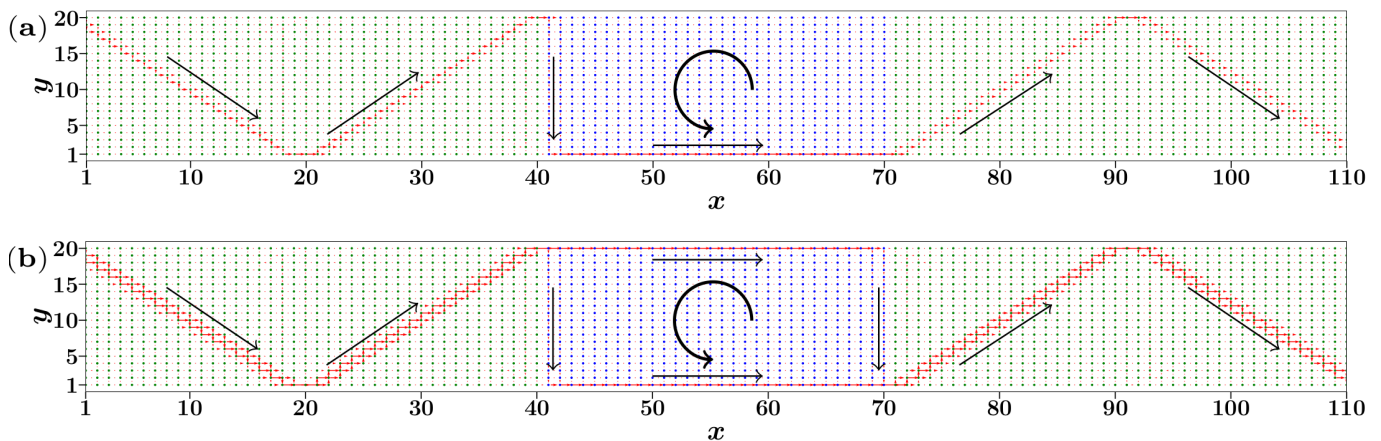


FIG. 3. Excess current density in the metallic leads and the SBHZ wire at zero Fermi level with (a) $\Delta\mu_R = 0$, $\Delta\mu_L > 0$ and (b) $\Delta\mu_L = -\Delta\mu_R = \Delta\mu$. The current in the reservoirs is localized along the lines at ± 45 degrees to the horizontal directions. The black straight arrows indicate the direction of the flow of the current and the curved arrow indicates the chirality of the CI. We see that in (b) the excess currents on the top and right edges of the CI flow opposite to its chirality. Parameter values: $N_x = 30$, $N_y = 20$, $\eta_b = \eta_c = 1$ and $\mu_w = 1$.

ical results of the effects of deforming the Fermi surface on the current density. The fact that the observed localization is sharp at $\mu = 0$ seems to suggest that it is very special to the scattering states formed by the edge modes of the insulator and the reservoir modes at zero energy. At zero energy, the Fermi surface in the metal is a square in momentum space. The localization arises from a particular superposition of the modes on this surface. To illustrate this, consider the setup in Fig. 4 where a current is injected into a semi-infinite metallic strip of width W at the left-bottom corner through a point contact with a 1D reservoir. The motivation for considering such a setup comes from the numerical observation (in Fig. (3)) that the current is injected near the corner into the metallic region. For simplicity, let the Hamiltonian of the 1D reservoir and the metallic strip be of the nearest neighbour tight-binding form, with all the hopping parameters, including that of the point contact at the corner, set to 1. At any lattice site (x, y) , the wave function components of the nearest neighbour points will sum to zero. In Fig 4, a solution is presented for one such scattering state with the wave function being non-zero only at certain points (large green circles). As $W \rightarrow \infty$, the solution can be written as a simple superposition of states on the square Fermi surface. This state displays a current localization similar to what we see numerically in Fig. (3b). The existence of such states at zero Fermi level and the current injection near the corners are the reasons for the observed localization of the current in the leads. In Sec. (V) of [21] we provide an argument for the observed corner injection/ejection in our numerics. We construct scattering states of the metal-CI junction in the limit $N_y \rightarrow \infty$ and show that there is no injection of current across the junction. Hence we infer that in the strip geometry there can be no injection of current in the

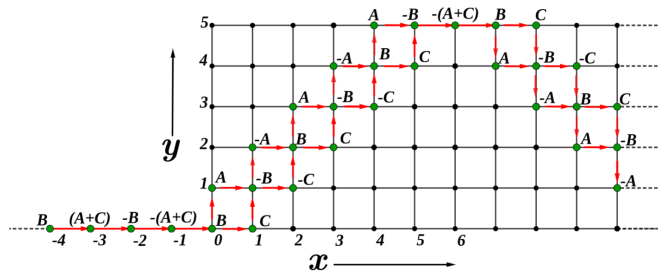


FIG. 4. A scattering state at zero energy in a 2D metallic strip with injection at the left bottom corner. The wavefunction is non-zero only on the green-marked sites, with the amplitudes indicated by A, B, C and their combinations. The red arrows indicate the currents.

bulk but only near the corners.

Topological quantities are expected to be robust to the effects of weak disorder. Hence a natural question to investigate is as to what happens to the current density patterns and the quantized two-terminal conductance on introducing contact disorder. We find features of the current density as well as the quantization are retained in the presence of disorder at the contacts (See Fig. (S6) in [21]).

Conclusion: We looked at electronic transport properties due to the edge modes of a Chern insulator (CI) in the open system geometry using a microscopic approach based on the NEGF formalism, applied to the spinless-BHZ model. We found very nontrivial effects on the current density pattern inside the leads arising from the topology of the insulator. Particularly, our numerical results indicate that the current is highly localized, both in the metal and in the insulator, and the injection (ejection) into (from) the insulator happens only near the

corners. The corner injection is robust to contact disorder and changes in the chemical potential. This provides a justification for the main assumption of LB, that of the emergence of an ideal point contact and consequently for the quantization of G . By the analysis of scattering states that are formed at metal-CI interfaces we have provided some analytic arguments that support our observations of the current patterns.

We also verified numerically that the two terminal longitudinal conductance in the open geometry is quantized and found very interesting finite-size effects. The conductance, at Fermi level $\mu = 0$, grows non-monotonically with increasing metal-CI coupling strength, η_c , and increasing transverse system size, N_y . The growth to the quantized value shows oscillations with a period that scales as $N_y^{1/2}\eta_c$.

Analytic proofs of the quantization of the two-terminal conductance and the emergence of the ideal point contact for a large class of models of insulators with non-trivial topology is desirable and remains an open problem. This would lead to an understanding of topology of open systems. The experimental observation of the current patterns and the finite size-effects are intriguing possibilities.

We thank Adhip Agarwala, Anindya Das, Sriram Ganeshan, Joel Moore, Arun Paramekanti and Diptiman Sen for helpful discussions. J.M.B and A.D. acknowledge the support of the Department of Atomic Energy, Government of India, under Project No. RTI4001.

-
- [1] K. v. Klitzing, G. Dorda, and M. Pepper, New method for high-accuracy determination of the fine-structure constant based on quantized hall resistance, *Phys. Rev. Lett.* **45**, 494 (1980).
- [2] D. J. Thouless, M. Kohmoto, M. P. Nightingale, and M. den Nijs, Quantized hall conductance in a two-dimensional periodic potential, *Phys. Rev. Lett.* **49**, 405 (1982).
- [3] Y. Hatsugai, Chern number and edge states in the integer quantum hall effect, *Phys. Rev. Lett.* **71**, 3697 (1993).
- [4] F. D. M. Haldane, Model for a quantum hall effect without landau levels: Condensed-matter realization of the "parity anomaly", *Phys. Rev. Lett.* **61**, 2015 (1988).
- [5] C.-Z. Chang, J. Zhang, X. Feng, J. Shen, Z. Zhang, M. Guo, K. Li, Y. Ou, P. Wei, L.-L. Wang, *et al.*, Experimental observation of the quantum anomalous hall effect in a magnetic topological insulator, *Science* **340**, 167 (2013).
- [6] G. Jotzu, M. Messer, R. Desbuquois, M. Lebrat, T. Uehlinger, D. Greif, and T. Esslinger, Experimental realization of the topological haldane model with ultracold fermions, *Nature* **515**, 237 (2014).
- [7] C. L. Kane and E. J. Mele, Z_2 topological order and the quantum spin hall effect, *Phys. Rev. Lett.* **95**, 146802 (2005).
- [8] B. A. Bernevig, T. L. Hughes, and S.-C. Zhang, Quantum spin hall effect and topological phase transition in hgte quantum wells, *Science* **314**, 1757 (2006).
- [9] R. Roy, Z_2 classification of quantum spin hall systems: An approach using time-reversal invariance, *Physical Review B* **79**, 195321 (2009).
- [10] R. Roy, Topological phases and the quantum spin hall effect in three dimensions, *Physical Review B* **79**, 195322 (2009).
- [11] L. Fu, C. L. Kane, and E. J. Mele, Topological insulators in three dimensions, *Phys. Rev. Lett.* **98**, 106803 (2007).
- [12] J. E. Moore and L. Balents, Topological invariants of time-reversal-invariant band structures, *Physical Review B* **75**, 121306 (2007).
- [13] M. König, S. Wiedmann, C. Brüne, A. Roth, H. Buhmann, L. W. Molenkamp, X.-L. Qi, and S.-C. Zhang, Quantum spin hall insulator state in hgte quantum wells, *Science* **318**, 766 (2007).
- [14] M. Z. Hasan and C. L. Kane, Colloquium: topological insulators, *Rev. Mod. Phys.* **82**, 3045 (2010).
- [15] H. Huang and F. Liu, Quantum spin hall effect and spin bott index in a quasicrystal lattice, *Phys. Rev. Lett.* **121**, 126401 (2018).
- [16] M. A. Bandres, M. C. Rechtsman, and M. Segev, Topological photonic quasicrystals: Fractal topological spectrum and protected transport, *Phys. Rev. X* **6**, 011016 (2016).
- [17] A. Agarwala and V. B. Shenoy, Topological insulators in amorphous systems, *Phys. Rev. Lett.* **118**, 236402 (2017).
- [18] Y. Tokura, M. Kawasaki, and N. Nagaosa, Emergent functions of quantum materials, *Nature Physics* **13**, 1056 (2017).
- [19] G. Gusev, Z. Kvon, E. Olshanetsky, and N. Mikhailov, Mesoscopic transport in two-dimensional topological insulators, *Solid State Commun.* **302**, 113701 (2019).
- [20] G. Dolcetto, M. Sasseti, and T. L. Schmidt, Edge physics in two-dimensional topological insulators, *La Rivista del Nuovo Cimento* **39**, 113 (2016).
- [21] Supplemental material, `URL_will_be_inserted_by_publisher`.
- [22] R. Shankar, Topological insulators—a review, *arXiv preprint arXiv:1804.06471* (2018).
- [23] A. Dhar and D. Sen, Nonequilibrium green's function formalism and the problem of bound states, *Phys. Rev. B* **73**, 085119 (2006).
- [24] J. M. Bhat and A. Dhar, Transport in spinless superconducting wires, *Phys. Rev. B* **102**, 224512 (2020).

Supplemental Material: Quantized longitudinal conductance and edge states in an open geometry 2-dimensional Chern insulator

Junaid Majeed Bhat¹, R Shankar², and Abhishek Dhar¹

¹International Centre for Theoretical Sciences, Tata Institute of Fundamental Research, Bengaluru 560 089, India

²The Institute of Mathematical Sciences, C I T Campus, Chennai 600 113, India

(Dated: January 15, 2024)

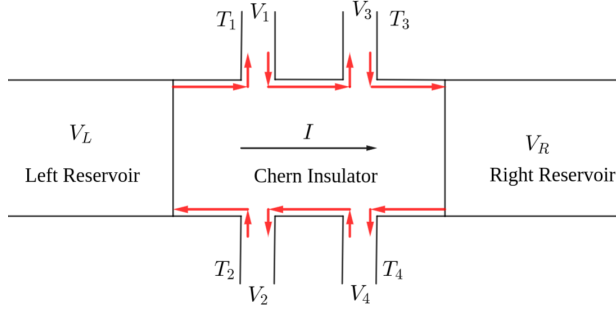


FIG. S1. 4-Terminal Hall bar setup.

I. EQUIVALENCE OF G AND G_H IN A 4-TERMINAL HALL BAR SETUP

Consider the 4-terminal hall bar setup shown in Fig. (S1). A current I flows through the insulator from the left to the right reservoir. The definitions of two-terminal conductance, G and the Hall conductance, G_H are given by $G = I/(V_L - V_R)$ and $G_H = I/(V_1 - V_2)$. Under Landauer-Buttiker formalism and assuming that the chirality of the CI to be clockwise (indicated by red arrows in Fig. (S1)), the currents flowing into the terminals T_1 , T_3 , T_4 and T_2 are given by,

$$\begin{aligned} I_1 &= \frac{e^2}{h}(V_1 - V_L), \quad I_3 = \frac{e^2}{h}(V_3 - V_1), \\ I_4 &= \frac{e^2}{h}(V_4 - V_R) \quad \text{and} \quad I_2 = \frac{e^2}{h}(V_2 - V_4). \end{aligned} \quad (\text{S1})$$

If no current is allowed to flow into the probes, we have $V_L = V_1 = V_3$, and $V_2 = V_4 = V_R$, which immediately imply $G = I/(V_L - V_R) = I/(V_1 - V_2) = G_H$. The quantization of G_H and G is straightforward as under the assumption of perfect transmission of the Landauer-Buttiker formalism we have $I = \frac{e^2}{h}(V_L - V_2) = \frac{e^2}{h}(V_L - V_R)$. This directly gives G_H as well as G to be quantized to e^2/h . Note that the longitudinal resistance defined as $R_L = (V_1 - V_3)/I$ vanishes, while $R_H = 1/G_H$ is non-zero, and this implies that the longitudinal conductance G_L also vanishes (on inverting the resistance matrix).

II. THE RESERVOIR HAMILTONIANS

We take two fermionic degrees of freedom on each site in the two reservoirs as well. We label the corresponding annihilation operators as $\psi_{1,L/R}(x_{L/R}, y)$ and

$\psi_{2,L/R}(x_{L/R}, y)$, where L and R label the left and the right lead, respectively. The integers x_L and x_R label the x coordinates of the sites on the left and the right reservoirs, respectively. These take integer values that run from $-\infty$ to 0 and $N_x + 1$ to ∞ , respectively. The y coordinate here takes the same integer values as in the wire (SBHZ insulator) i.e. from 1 to N_y . Free boundary conditions are imposed at the edges of the reservoir and the system at $y = 1$ and $y = N_y$ respectively. The full Hamiltonian of the system and baths is therefore given by:

$$\mathcal{H} = \mathcal{H}_L + \mathcal{H}_{WL} + \mathcal{H}_W + \mathcal{H}_{WR} + \mathcal{H}_R. \quad (\text{S2})$$

where \mathcal{H}_W is the Hamiltonian of the SBHZ CI and

$$\mathcal{H}_W = \sum_{x,x'=1}^{N_x} \sum_{y,y'=1}^{N_y} \Psi^\dagger(x, y) \mathcal{H}_W[x, y; x', y'] \Psi(x', y') \quad (\text{S3a})$$

$$\begin{aligned} &= \sum_{x=1}^{N_x} \sum_{y=1}^{N_y} \mu_w \Psi^\dagger(x, y) \sigma_z \Psi(x, y) \\ &+ \sum_{x=1}^{N_x-1} \sum_{y=1}^{N_y} \left[\Psi^\dagger(x, y) \frac{1}{2} (\sigma_z + i\sigma_x) \Psi(x+1, y) + \text{h.c.} \right] \\ &+ \sum_{x=1}^{N_x} \sum_{y=1}^{N_y-1} \left[\Psi^\dagger(x, y) \frac{1}{2} (\sigma_z + i\sigma_y) \Psi(x, y+1) + \text{h.c.} \right], \end{aligned}$$

$$\mathcal{H}_{WL} = \sum_{x_L=-\infty}^0 \sum_{x=1}^{N_x} \sum_{y,y'=1}^{N_y} \left[\Psi_L^\dagger(x_L, y) V_L[x_L, y; x, y'] \Psi[x, y'] + \text{h.c.} \right] \quad (\text{S3b})$$

$$= \eta_c \sum_{y=1}^{N_y} \left[\Psi_L^\dagger(0, y) \Psi(1, y) + \text{h.c.} \right],$$

$$\mathcal{H}_{WR} = \sum_{x_R=N_x+1}^{\infty} \sum_{x=1}^{N_x} \sum_{y,y'=1}^{N_y} \left[\Psi_R^\dagger(x_R, y) V_R[x_R, y; x, y'] \Psi[x, y'] + \text{h.c.} \right] \quad (\text{S3c})$$

$$= \eta_c \sum_{y=1}^{N_y} \left[\Psi_R^\dagger(N_x + 1, y) \Psi(N_x, y') + \text{h.c.} \right],$$

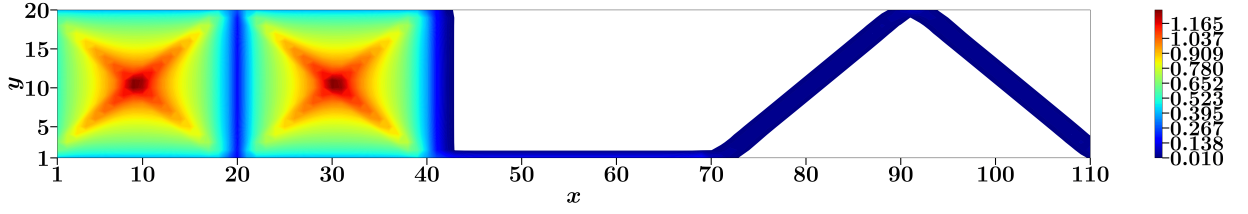


FIG. S2. Excess charge in the leads and the SBHZ wire at zero Fermi level. Deep inside the insulator (white region), the density has a value less than 10^{-8} . Parameter values $-N_x \times N_y = 30 \times 20$, $\Delta\mu_R = 0$, $\eta_b = \eta_c = 1$ and $\mu_w = 1$.

$$\mathcal{H}_L = \sum_{x_L, x'_L = -\infty}^0 \sum_{y=1}^{N_y} \Psi_L^\dagger(x_L, y) H_L[x_L, y; x'_L, y'] \Psi_L(x'_L, y') \quad (\text{S3d})$$

$$= \eta_b \sum_{x_L = -\infty}^{-1} \sum_{y=1}^{N_y} \left[\Psi_L^\dagger(x_L, y) \Psi_L(x_L + 1, y) + \text{h.c.} \right] \\ + \eta_b \sum_{x_L = -\infty}^0 \sum_{y=1}^{N_y-1} \left[\Psi_L^\dagger(x_L, y) \Psi_L(x_L, y + 1) + \text{h.c.} \right],$$

$$\mathcal{H}_R = \sum_{x_R, x'_R = N_x+1}^{\infty} \sum_{y=1}^{N_y} \Psi_R^\dagger(x_R, y) H_R[x_R, y; x'_R, y'] \Psi_R(x'_R, y') \quad (\text{S3e})$$

$$= \eta_b \sum_{x_R = N_x+1}^{\infty} \sum_{y=1}^{N_y} \left[\Psi_R^\dagger(x_R, y) \Psi_R(x_R + 1, y) + \text{h.c.} \right] \\ + \eta_b \sum_{x_R = N_x+1}^{\infty} \sum_{y=1}^{N_y-1} \left[\Psi_R^\dagger(x_R, y) \Psi_R(x_R, y + 1) + \text{h.c.} \right],$$

where $\Psi_{L/R}(x, y) = (\psi_{1,L/R}(x, y) \ \psi_{2,L/R}(x, y))^T$, η_b is the hopping strength between the sites in the reservoir, and η_c is the coupling between the CI and the reservoirs.

III. NEGF RESULTS FOR CURRENT AND CHARGE DENSITY

Here we present the details of the expressions for current and charge densities from the NEGF formalism. From Ref. [23, 24] of the main text, the expression for the correlation matrix C with components defined as $C_{\mathbf{x}, \mathbf{x}'; a, b} = \langle \psi_a^\dagger(\mathbf{x}) \psi_b(\mathbf{x}') \rangle$ ($a, b = 1, 2$ and $\mathbf{x} = (x, y)$),

$$C = \int_{-\infty}^{\infty} d\omega [C^L(\omega) f(\omega, \mu_L, T_L) + C^R(\omega) f(\omega, \mu_R, T_R)], \quad (\text{S4})$$

where $f(\omega, \mu, T)$ is the Fermi Dirac distribution function, $C^{L/R}(\omega) = 2\pi \mathcal{G}^+(\omega) \Gamma_{L/R}(\omega) \mathcal{G}^-(\omega)$. $\mathcal{G}^+(\omega)$ is the

effective Green's function of the wire given by $\mathcal{G}^+(\omega) = (\omega - H_W - \Sigma_L(\omega) - \Sigma_R(\omega))^{-1}$ where $\Sigma_{L/R}(\omega) = V_{L/R}^\dagger (\omega - H_{L/R})^{-1} V_{L/R}$ are the self energy contributions due to the reservoirs. The charge density and the current density are given terms of C as follows:

$$\rho(\mathbf{x}) = \sum_{a=1}^2 C_{\mathbf{x}, a; \mathbf{x}, a}, \quad (\text{S5})$$

$$J_{\mathbf{x}, \mathbf{x}'} = -2 \sum_{a, b=1}^2 \text{Im} \left[H_W[\mathbf{x}, a; \mathbf{x}', b] C_{\mathbf{x}, a; \mathbf{x}', b} \right]. \quad (\text{S6})$$

$J_{\mathbf{x}, \mathbf{x}'}$ is the net particle current on the bond between the lattice points \mathbf{x} and \mathbf{x}' . Clearly, it is zero if the two are not nearest neighbours on the square lattice.

For $T_L = T_R = 0$, $\mu_L = \mu + \Delta\mu_L$ and $\mu_R = \mu + \Delta\mu_R$ with $\Delta\mu_L, \Delta\mu_R \ll \mu$, the expressions for the current density can be simplified and split into the equilibrium part, J^{eq} and the excess part, \bar{J} . The equilibrium part is the current density for $\Delta\mu_L = \Delta\mu_R = 0$ and is given by

$$J_{\mathbf{x}, \mathbf{x}'}^{eq} = \int_{-\infty}^{\mu} d\omega [F_{\mathbf{x}, \mathbf{x}'}^L(\omega) + F_{\mathbf{x}, \mathbf{x}'}^R(\omega)], \quad (\text{S7})$$

where

$$F_{\mathbf{x}, \mathbf{x}'}^{L/R}(\omega) = -2 \sum_{a, b=1}^2 \text{Im} \left(H_W[\mathbf{x}, a; \mathbf{x}', b] C_{\mathbf{x}, a; \mathbf{x}', b}^{L/R}(\omega) \right). \quad (\text{S8})$$

The excess current, \bar{J} , is the first order correction to J^{eq} and can be written as $\bar{J} = \bar{J}_L + \bar{J}_R$ where $\bar{J}_{\mathbf{x}, \mathbf{x}'}^{L/R} = F_{\mathbf{x}, \mathbf{x}'}^{L/R}(\mu) \Delta\mu_{L/R}$.

A similar algebra gives the excess charge density to be,

$$\bar{\rho}(x, y) = \sum_{a=1}^2 C_{\mathbf{x}, a; \mathbf{x}, a}^L(\mu) \Delta\mu_L + C_{\mathbf{x}, a; \mathbf{x}', a}^R(\mu) \Delta\mu_R. \quad (\text{S9})$$

We show in Fig. S2 the excess charge density with $\Delta\mu_L >$

0 and $\Delta\mu_R = 0$. We see that the excess charge from the

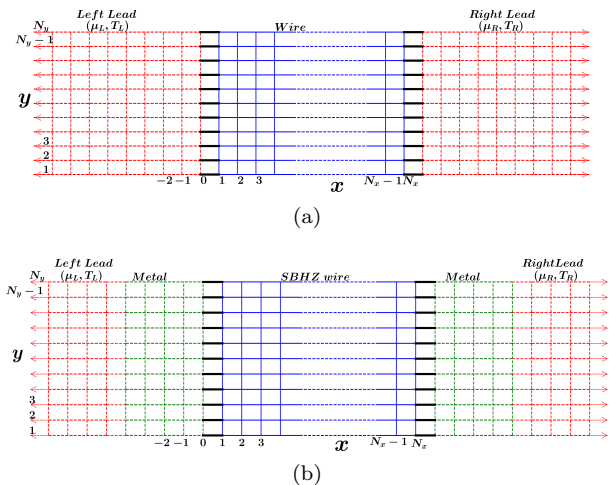


FIG. S3. Schematic of two geometries used for the calculation of the current density in the SBHZ wire and the reservoirs. The red regions are the reservoirs. The green region is the normal metallic region with a Hamiltonian identical to the reservoirs. The blue region is the SBHZ wire. The microscopic Hamiltonian for the two geometries is exactly the same and the two only differ in the initial condition, namely the red regions where the temperatures and chemical potentials are specified differ in the two geometries.

left lead gets distributed into the right lead along the lines of localization of the excess current.

While Eq. (S5) and Eq. (S6) gives us the charge and the current density inside the system, these can also be used to compute the current density in the leads with a slight modification of H_W . The main point to note is that in the NESS of the full system and reservoirs, the state inside the reservoirs has also evolved and in fact contains information about the scattering states (plane waves incident from either reservoir onto the scattering region formed by

the insulator). We thus consider a setup (see Fig (S3b)) that consists of the CI (blue region) sandwiched between finite metallic segments (green region), which are in turn connected to the metallic reservoirs (red region). Compared to the original setup in Fig (S3a), the new setup now includes parts of the lead Hamiltonians (green region) inside the system Hamiltonian, H_W . Therefore, we can now use the NEGF formalism to compute current everywhere inside the system, including the green metallic sites. The current density in any finite segment of the two setups in Fig (S3) is identical because of uniqueness of the NESS.

IV. EFFECTS OF THE SHAPE OF THE FERMI SURFACE AND DISORDER

If the Fermi surface is slightly deformed, the features of the current density, namely the corner ejection and injection and localization inside the reservoirs, are retained up to slight perturbations. To illustrate this, we consider deforming the Fermi level in two ways: (a) tuning the Fermi level of the reservoirs away from zero and (b) introducing anisotropy inside the reservoirs while keeping the Fermi level at zero. Fig. (S4) shows the current density at $\mu = 0.2$. The localization of the current disappears deep in the metallic region, however, the corner injection and ejection is retained.

We introduce anisotropy in the reservoirs by choosing different hoppings in the x and y directions, respectively. The results are shown in Fig. (S5), where we plot the current densities for $\eta_{by} = 1.1$, $\eta_{by} = 1.2$ and $\eta_{by} = 1.3$ with $\eta_{bx} = 1$. While the injection/ejection is still near the corners, the localization feature is retained for small perturbations but slowly gets washed away for increased anisotropy. Interestingly, on changing η_{by} , the angle of the lines with the x -axis also gets changed from 45 degrees.

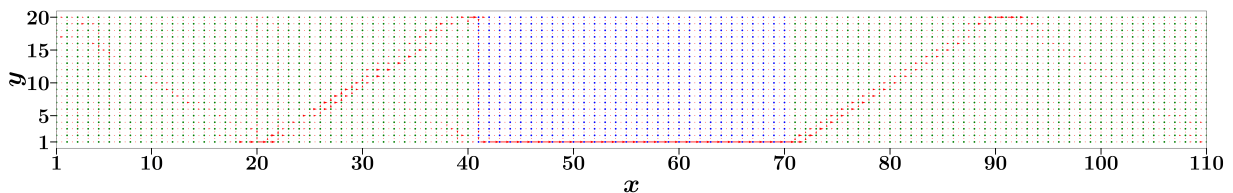


FIG. S4. Excess current density, $\bar{J}/\Delta\mu_L$, in the reservoirs and the SBHZ wire with $\mu = 0.2$. The current in the reservoirs is localized along the lines at 45 degrees to the horizontal directions. Parameter values- $N_x \times N_y = 30 \times 20$, $\Delta\mu_R = 0$, $\eta_b = \eta_c = 1$ and $\mu_w = 1$.

We also look at the effect of contact disorder between the insulator and the reservoirs on the observed features of the current. We show the results in Fig. S6 where the coupling parameters between the system and the reser-

voir are chosen randomly. We see that features of the current are almost unaffected by the disorder. Therefore, to a certain degree, the observed effects enjoy topological protection of the edge modes.

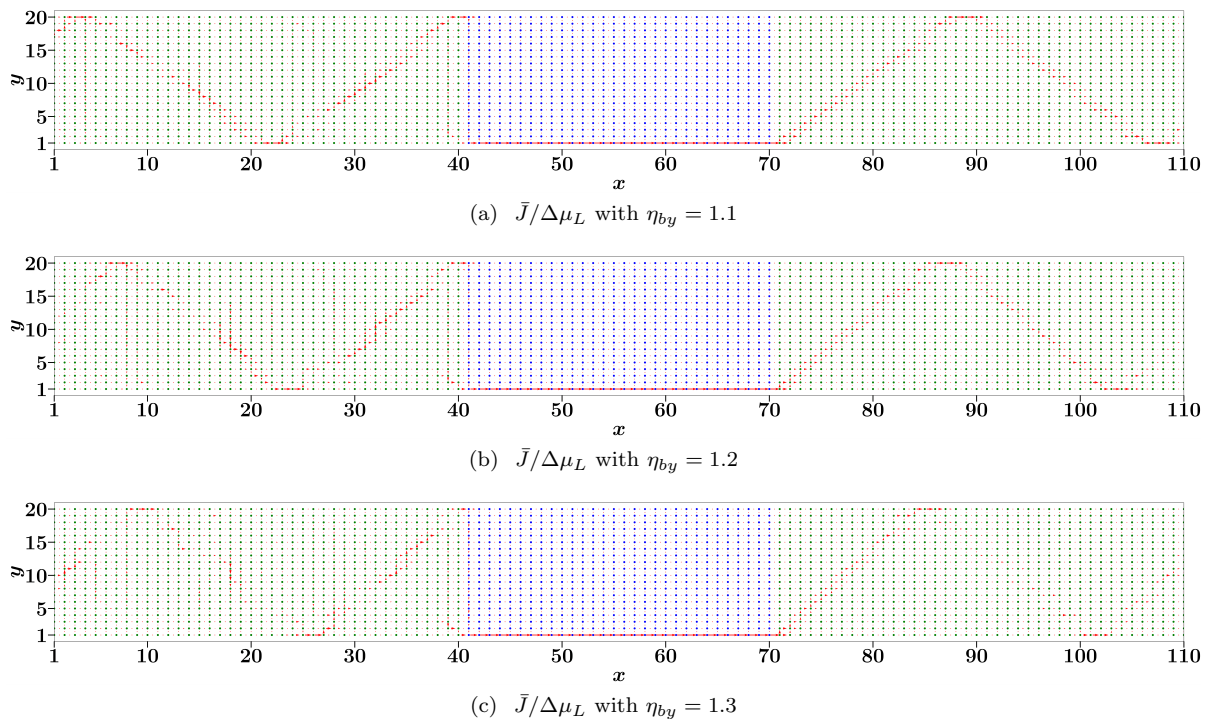


FIG. S5. Excess current density in the an-isotropic reservoirs and the SBHZ wire. The anisotropy is introduced by choosing different hopping, denoted by η_{bx} and η_{by} , in the x and y directions respectively. The current in the reservoirs is localized along the lines at 45 degrees to the horizontal directions. Parameter values— $N_x = 30$, $N_y = 20$, $\Delta\mu_R = 0$, $\eta_{bx} = \eta_c = 1$, $\mu = 0$ and $\mu_w = 1$.

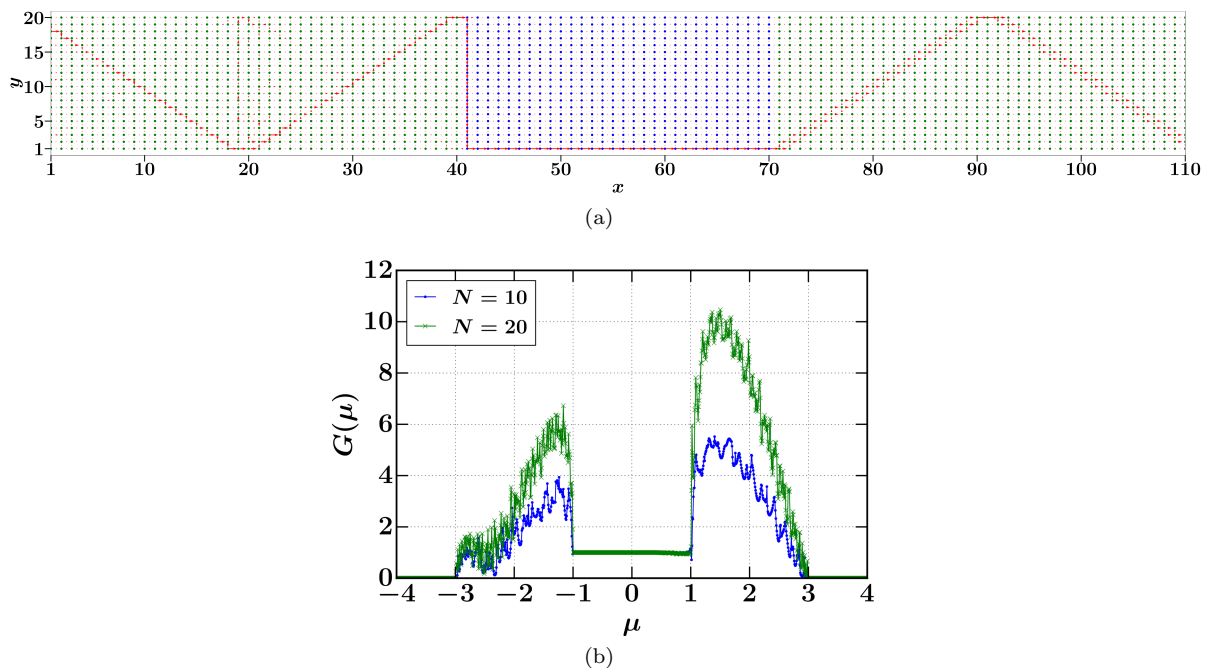


FIG. S6. (a) Excess current density in the reservoirs and the SBHZ wire with disordered contacts. The disorder at the contacts is introduced by choosing the coupling, η_c , at every bond random from the interval $(0.75, 1.25)$. (b) shows the effect of disorder on the quantization of the two terminal conductance where the coupling, η_c is chosen randomly in the interval $(1, 2)$. Parameter values for (a) $N_x \times N_y = 30 \times 20$, $\Delta\mu_R = 0$, $\eta_{bx} = 1$, $\mu = 0$ and $\mu_w = 1$ and for (b) $N_x = N_y = N$, $\eta_b = 2$.

V. METAL-CHERN INSULATOR JUNCTION

by constructing an explicit solution for the wave func-

In this section, we show that there is no injection from the metallic leads inside the bulk of the Chern Insulator

tions at zero energy in the limit $N_y \rightarrow \infty$. To simplify the problem, we ignore the right lead and consider only the left metallic lead in contact with the SBHZ Chern insulator with $N_y \rightarrow \infty$. The Hamiltonian for the metallic

sites is chosen to be the same as the left reservoir with all the hoppings set to one. The equation for the eigenstates of zero energy away from the junction between the metal and CI are given by,

$$\Psi_M(x+1, y) + \Psi_M(x-1, y) + \Psi_M(x, y+1) + \Psi_M(x, y-1) = 0; \quad x \leq -1, \quad (\text{S10})$$

$$\frac{\sigma_z - i\sigma_x}{2}\Psi(x-1, y) + \frac{\sigma_z + i\sigma_x}{2}\Psi(x+1, y) + \mu_w\sigma_z\Psi(x, y) + \frac{\sigma_z - i\sigma_y}{2}\Psi(x, y-1) + \frac{\sigma_z + i\sigma_y}{2}\Psi(x, y+1) = 0; \quad x \geq 2, \quad (\text{S11})$$

where $\Psi_M(x, y)$ and $\Psi(x, y)$ are the two component wave functions in the metal and inside the Chern insulator, respectively. Using the translation symmetry in the y -direction, we can substitute

$$\Psi_M(x, y) = e^{iky}\Phi_M(x), \quad \text{and} \quad (\text{S12})$$

$$\Psi(x, y) = e^{iky}\Phi(x), \quad (\text{S13})$$

into the Eq. (S10) and Eq. (S11), respectively. This gives the equation for $\Phi_M(x)$ and $\Phi(x)$ to be,

$$\Phi_M(x+1) + \Phi_M(x-1) + 2\cos k\Phi_M(x) = 0, \quad (\text{S14})$$

$$\begin{aligned} & \frac{\sigma_z - i\sigma_x}{2}\Phi(x-1) + \frac{\sigma_z + i\sigma_x}{2}\Phi(x+1) \\ & + \left[\mu_w\sigma_z + \frac{\sigma_z - i\sigma_y}{2}e^{-ik} + \frac{\sigma_z + i\sigma_y}{2}e^{ik} \right] \Phi(x) = 0. \end{aligned} \quad (\text{S15})$$

The zero energy solution inside the Chern insulator is localized so we substitute,

$$\Phi(x) = \begin{pmatrix} u \\ v \end{pmatrix} z^{x-1}, \quad (\text{S16})$$

in Eq. S15 and look for solution with $|z| < 1$. This gives the equation for u, v to be $M \begin{pmatrix} u \\ v \end{pmatrix} = 0$, where

$$M = \begin{pmatrix} \frac{1}{2}(z + \frac{1}{z}) + \mu_w + \cos k & \frac{i}{2}(z - \frac{1}{z}) + i \sin k \\ \frac{i}{2}(z - \frac{1}{z}) - i \sin k & -(\frac{1}{2}(z + \frac{1}{z}) + \mu_w + \cos k) \end{pmatrix}. \quad (\text{S17})$$

For a non-trivial solution we have $\det[M] = 0$ which gives two solutions for z ,

$$z_{\pm}(k) = -\alpha(k) \pm \sqrt{\alpha^2(k) - 1}; \quad \alpha(k) = \frac{\mu_w^2 + 2\mu_w \cos k + 2}{2(\mu_w + \cos k)}. \quad (\text{S18})$$

Clearly, $z_+z_- = 1$, so we choose the one with $|z| < 1$ which for now we assume to be z_+ . Using this we have for $u = \beta(k)v$ where,

$$\beta(k) = -\frac{-\alpha(k) + \mu_w + \cos k}{i(\sqrt{\alpha^2(k) - 1} + \sin k)}. \quad (\text{S19})$$

We can now write the full solution for the wave function at zero energy for the system as follows:

$$\Phi_M(x) = e^{ik_x(x-1)} \begin{pmatrix} 1 \\ B \end{pmatrix} + e^{-ik_x(x-1)} \begin{pmatrix} r_1 \\ r_2 \end{pmatrix}, \quad (\text{S20})$$

$$\Phi(x) = \begin{pmatrix} u \\ \beta(k)u \end{pmatrix} z^{x-1}, \quad (\text{S21})$$

where B is the amplitude of the incoming electron wave, and r_1, r_2 are its reflection coefficients onto the two degrees of freedom in the metal, respectively. To satisfy Eq. (S14) inside the metal we take $k_x = k + \pi$. The coefficients B, r_1, r_2 , and u are chosen so that they satisfy the equations near the junction at $x = 0$ and $x = 1$. From the equations at these two values of x , we would basically get four linear equations for u, B, r_1 and r_2 . We have at $x = 0$,

$$\Phi_M(-1) + 2\cos k\Phi_M(0) + \eta_c\Phi(1) = 0, \quad (\text{S22})$$

$$\implies -\Phi_M(1) + \eta_c\Phi(1) = 0. \quad (\text{S23})$$

While going from Eq. S22 to Eq. S23, we used the fact that sum of the first, the second term in Eq. (S22) and $\Phi_M(x)$ evaluated at $x = 1$ vanishes. We now have two linear equations for the coefficients r_1, r_2, B and u . To obtain the other two equations, we consider the equation for the site at $x = 1$. This is given by

$$\begin{aligned} & \eta_c\Phi_M(0) + \frac{\sigma_z + i\sigma_x}{2}\Phi(2) \\ & + \left[\mu_w\sigma_z + \frac{\sigma_z - i\sigma_y}{2}e^{-ik} + \frac{\sigma_z + i\sigma_y}{2}e^{ik} \right] \Phi(1) = 0, \end{aligned} \quad (\text{S24})$$

$$\implies \eta_c\Phi_M(0) - \left(\frac{\sigma_z - i\sigma_x}{2} \right) \Phi(0) = 0. \quad (\text{S25})$$

Eq. (S25) follows from the Eq. (S24) by noting that the sum of the second term, the third term in Eq. (S24) and the term $(1/2)(\sigma_z - i\sigma_x)\Phi(0)$ vanishes. We therefore have the following linear equations for the coefficients $B, r_1,$

r_2 , and u from Eq. (S23) and Eq. (S25):

$$\begin{pmatrix} 0 & -1 & 0 & \eta_c \\ -1 & 0 & -1 & \beta\eta_c \\ 0 & -\eta_c e^{ik} & 0 & -g \\ -\eta_c e^{-ik} & 0 & -\eta_c e^{ik} & ig \end{pmatrix} \begin{pmatrix} B \\ r_1 \\ r_2 \\ u \end{pmatrix} = \begin{pmatrix} 1 \\ 0 \\ \eta_c e^{-ik} \\ 0 \end{pmatrix}, \quad (\text{S26})$$

where $g = (1 - i\beta)/(2z_+)$. From this linear system, the solution for the coefficients is given by,

$$\begin{pmatrix} B \\ r_1 \\ r_2 \\ u \end{pmatrix} = \begin{pmatrix} \beta - \frac{g(i+\beta)}{g+\eta_c^2 e^{ik}} \\ -\frac{g+\eta_c^2 e^{-ik}}{g+\eta_c^2 e^{ik}} \\ \frac{ig-\beta\eta_c^2 e^{-ik}}{g+\eta_c^2 e^{ik}} \\ \frac{2i\eta_c \sin k}{g+e^{ik}\eta_c^2} \end{pmatrix}. \quad (\text{S27})$$

The current flowing in the x -direction from $x = 0$ and $x = 1$ between the first degree of freedom on the two sites is given by,

$$J_x^{11} = -2I\eta_c [\Phi^{*1}(1)\Phi_M^1(0) - \Phi^1(1)\Phi_M^{*1}(0)], \quad (\text{S28})$$

where the superscript 1 on $\Phi(0)$ and $\Phi_M(-1)$ refers to the first component of these two vectors. On simplification the current gives,

$$\begin{aligned} J_x^{11} &= -2i\eta_c (u^* (-e^{-ik} - e^{ik}r_1) - \text{c.c.}), \quad (\text{S29}) \\ &= \frac{-8i\eta_c^2}{|g + e^{ik}\eta_c|^2} (g - g^*) = 0, \quad (\text{S30}) \end{aligned}$$

as g is real. A similar calculation gives the current flowing between the other two degrees of freedom J_x^{22} to be zero. Therefore, there is no injection from the metal into the CI. From this we infer that in the strip geometry the injection should take place only near the corners.

We now look at the current in the y -direction at $x = 1$ on the edge of the CI. This is given by

$$J_y = -2i(\Psi^\dagger(x, y) \frac{1}{2}(\sigma_x - i\sigma_y)\Psi(x, y+1) - \text{c.c.}) \quad (\text{S31})$$

where $\Psi(x, y)$ is given by Eq. (S13). On simplification this gives a non-zero current,

$$J_y = 8\eta_c^2 \frac{(1 + \beta^2) \sin k - 2\beta \cos k}{|g + \eta_c^2 e^{ik}|^2} \sin^2 k, \quad (\text{S32})$$

which flows along the edge of the CI.

While the solution given in Eq. (S20) and Eq. (S21) with the coefficients given by Eq. (S27) is a valid solution, this is not the only possible solution at a particular value of k . There exists another linearly independent solution for the same k . To see this, we consider a solution in the Chern insulator such that $(\sigma_z - i\sigma_x)\Phi(1) = 0$. This condition makes $\Phi(1)$ vanish from the equations inside the Chern insulator. Therefore, the solution of the form chosen in Eq. (S16) is no longer valid for $x = 1$. Hence, at $x = 1$ we are free to choose $\Phi(1) = \begin{pmatrix} 1 \\ -i \end{pmatrix} \tilde{u}$, and for $x \geq 2$ the solution is still described by the ansatz in Eq. (S16). At the boundaries, we now have four equations given by Eq. (S23) and Eq. (S24). For this case, Eq. (S24) should be used at the boundaries not Eq. (S25). The latter is no longer true as $\Phi(1)$ is no longer given by the ansatz in Eq. (S16). We therefore have four equations at the boundaries but five variables given by B , r_1 , r_2 , \tilde{u} and u . The extra degree of freedom implies two linearly independent solutions for each k . If we choose $\tilde{u} = u$, then we get the solutions derived earlier with $\beta(k) = -i$. Another choice is to set $u = 0$, then the equations at the junction give the following solution for the remaining coefficients,

$$\begin{pmatrix} B \\ r_1 \\ r_2 \\ u \end{pmatrix} = \begin{pmatrix} -i \left(1 - \frac{g_- + g_+}{g_+ - \eta_c^2 e^{ik}} \right) \\ -\frac{g_+ - \eta_c^2 e^{-ik}}{g_+ - \eta_c^2 e^{ik}} \\ i \frac{(g_- + \eta_c^2 e^{-ik})}{g_+ - \eta_c^2 e^{ik}} \\ \frac{-2\eta_c \sin k}{g_+ - \eta_c^2 e^{ik}} \end{pmatrix}, \quad (\text{S33})$$

where $g_\pm = \mu_w + \cos k \pm \sin k$. A similar calculation as earlier gives that at the junction the current in the x -direction vanishes while simultaneously the current in the y -direction is nonzero.